Cui et al. Journal of Wood Science (2022) 68:17
https://doi.org/10.1186/s10086-022-02025-6

Journal of Wood Science

ORIGINAL ARTICLE Open Access

Spatial distribution characteristics of the dust emitted at different cutting speeds during MDF milling by image analysis

Yunqi Cui, Jian Yin, Yitong Cai, Huimin Wang, Nanfeng Zhu and Tao Ding*

Abstract

Wood dust produced in medium-density fiberboard (MDF) processing is a major occupational hazard in wood industry and may damage processing equipment. In many wood processing factories, dust collecting systems need to be optimized for the distributional and morphological characteristics of dust in the workshop so that economical and efficient dust control can be achieved. In this study, weighting, image analysis and scanning electron microscopy (SEM) were applied to explore the effects of different cutting speeds on the distribution and morphology of dust generated in MDF milling. The results showed that most dust particles were less than 100 μm and that the aspect ratios (AR) were between 0.6 and 0.7. There was significant difference in particle number size distribution (PNSD) between the dust at different sampling positions. Less amount of dust was located close to cutting center, and fine dust was more likely to appear far away from cutting center. Cutting speed was associated with PNSD, but had little effect on AR. The findings provide spatial distribution characteristics of MDF dust during milling, which can be helpful for optimizing cutting parameters and locating dust collecting hoods to minimize dust exposure.

Keywords: MDF dust, Milling, Cutting speed, Average chip thickness, Spatial distribution, Image analysis, Particle size, Aspect ratio

Introduction

Medium-density fiberboard (MDF) is an important wood-based panel product in wood industry, which is mainly composed of lingo-cellulosic fibers often bound together with urea–formaldehyde resin [1]. It has been widely applied in the manufacturing of furniture, cabinet and wall panel owing to its smooth surface and uniform edge [2]. The Food and Agriculture Organization (FAO) 2018 survey reported that the global output of MDF surpassed 99 million m^3, more than half of which was contributed by China alone [3]. However, massive quantities of dust are generated when MDF is being cut and milled in industrial woodworking. A recent study found that the amount of dust produced during MDF milling reached up to 30 times of that in pine milling, which was far higher than the fold number of 6, as reported in an earlier research [4].

Wood dust presents potential safety risks like fire, explosion, etc. [5, 6]. Excessive exposure to MDF dust can also cause great harm to human health [7]. Some studies have demonstrated that there is a strong association between wood dust and various respiratory diseases like asthma, chronic bronchitis, nasal symptoms, and chronic impairment in lung function [8]. It has been issued by the International Agency for Research on Cancer that wood dust is one of carcinogens to induce nasal and paranasal sinus malignancies according to extensive epidemiological evidences [9]. Meanwhile, wood dust can also affect the performance stability of milling machining center if it is not cleaned in time and accumulated in the machine. This probably causes disordered operation and short circuit of electronic components, leading to abnormal wear of the equipment inducing the increase of maintenance

*Correspondence: tao_ding@njfu.edu.cn
Nanjing Forestry University, 159 Longpan Rd., Nanjing 210037, China

costs and the decrease of equipment life span, and the damage to product quality [10, 11].

The most effective way to minimize dust emission is directly reducing the dust generated in milling operation by optimizing cutting parameters especially for the milling apparatus not suitable for the installation of dust collecting hoods [12]. Among these factors, the cutting speed of milling cutter is the most crucial factor, which significantly affects spatial distribution characteristics of the dust in workshop. Thus, it is necessary to explore the impacts of cutting speed on the shape and flowability of MDF dust in milling.

Morphological characteristics including particle size distribution (PSD) and shape distribution are the fundamental factors influencing dust handling behaviors such as flowability, bulk density and compressibility, etc. [13, 14]. Ockajova et al. analyzed the factors affecting the granularity of wood sanding dust and considered the proportion of dust smaller than 80 μm in diameter is 89.21%–96.29% [15, 16]. Mazumder found that the aerodynamic diameter of most MDF dust particles was less than 10 μm [17]. Some reports found that the morphology tended to be more uniform with the decrease of particle size [18, 19]. Saad et al. used roundness, aspect ratio, convexity and filling rate to characterize the morphology of wheat grinding powder and found that small particles had more regular morphology than large particles [20]. However, the distribution of irregularly shaped wood particles in space has been rarely studied, and in particular limited studies have been performed on size and shape characteristics and spatial distribution of MDF milling dust.

In the study, spindle rotation speed in milling operation was set as the main variable, and then spatial distribution and morphological characteristics of MDF dust at the same height as the cutting plane were detected for qualitative description and quantitative analysis. Flatbed scanning image analysis was utilized to measure particle number size distribution (PNSD) and aspect ratio (AR) of MDF dust [21, 22]. Scanning electron microscopy (SEM) was used as a direct assay to check dust morphological characteristics.

Experimental

Materials

MDF panels taken from Aiwei Industrial Development Co., Ltd, Shanghai, China, was cut apart for preparing workpieces with geometric dimension of 1000 mm × 300 mm × 18 mm (length × width × depth) as shown in Fig. 1a. The modulus of elasticity (MOE) and modulus of rupture (MOR) of the workpieces were 4185 MPa and 46.8 MPa, respectively. The moisture content (MC) was between 8.7% and 10.4%, and the average density was 675.3 kg/m^3. The 8-mm-diameter straight shank solid carbide milling cutter with 3 edges (Huhao Technology Co., Ltd, Hangzhou, China) and the milling machine (MGK01, Nanxing Machinery Co., Ltd, Dongguan, China) were used for milling operation in the

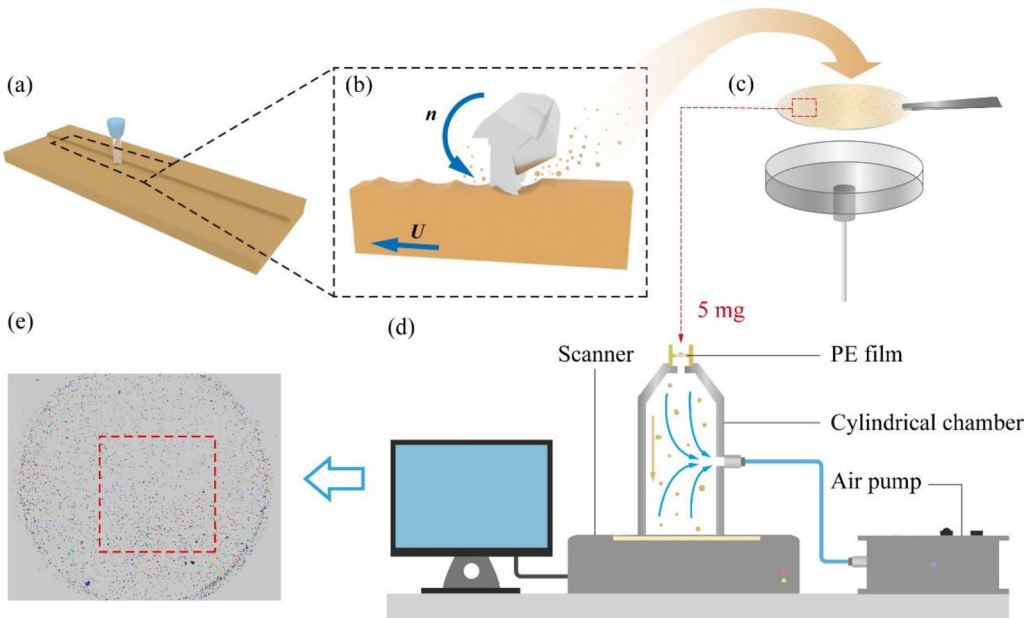

Fig. 1 Flowchart of dust sampling and scanning. **a** Diagram of MDF milling; **b** up-milling; **c** an acrylic disc held by a round dish was used to collect the falling dust in MDF milling at each sampling point; **d** flatbed scanning image analysis devices; **e** dust image

workshop with the initial temperature of 24 ± 1 ℃ and relative humidity (RH) of 60 ± 1%.

Cutting methods

Background dust concentration was adjusted around 0.07 mg/m^3 by measuring initial dust concentration in the room before each milling. As shown in Fig. 1b, the cutter was rotated counterclockwise during milling while the workpiece fixed on the bench by a vacuum chuck was fed against the direction of cutter rotation. The cutting parameters are shown in Table 1, the spindle speed was set at 8000, 12,000 and 16,000 rpm, and the corresponding cutting speed was 3.351 m/s, 5.027 m/s and 6.702 m/s, respectively. Actually, cutter rotation affects the formation of wood chips with different thickness when milling MDF. No matter how cutting parameters are set up, the thickness of wood chip exerts a decisive effect on the amount of dust [4, 23]. Average particle size and median diameter of PSD for MDF milling dust are elevated with the increase of average chip thickness [10]. Meanwhile, Rautio's study [23] indicated that the amount of airborne dust was increased strongly when chip thickness was lower than 0.05 mm. To generate more dust and exclude the interference caused by different chip thickness, average cutting thickness for all of three groups in our experiments was set as 0.05 mm. Therefore, the feed rate was adjusted according to the following Eq. 1:

$$u = \frac{h_{\mathrm{m}} nz}{1000}\sqrt{\frac{D}{h}} (\text{for } h \ll D), \tag{1}$$

where u is the feed rate (m/min), h_{m} is the average chip thickness (mm), n is the rotation rate (r/min), z is the number of milling edges on the tool, h is the milling depth (mm) and D is the tool diameter (mm). The feed rates of three groups were 3.394 m/min, 5.091 m/min and 6.788 m/min, respectively.

To ensure similar dust amount in total, the depth and width of cutting in the three groups was kept consistent, and the total volume for each group was 3 mm × 1000 mm × 300 mm. The dust collection was kept 4 h after milling till the dust in the air was reduced to the initial level before cutting, which meant the dust generated in milling basically fell down to the ground rather than floated in the air. The falling dust was collected using an acrylic disc with a diameter of 100 mm (Fig. 1c), which was then weighed and analyzed by flatbed scanning, etc. (Fig. 1d–e).

Sampling places

MDF workpiece was placed on the horizontal plane 0.7 m above the ground, and XOY coordinate system was established by marking the center of the plate as the origin 0. Twelve sampling lines were arranged along the X-axis direction at an interval of 0.5 m, which was labeled as A to L, respectively. Likewise, 7 sampling lines marked as A'–G' was distributed parallel to Y-axis direction. Then sampling points were located at the cross points of these lines. Dust mass around the cutting center changed rapidly, and 6 more sampling points are added near the cutting center including (− 0.25, − 0.5), (0.25, 0.5), (− 0.25, 0), (0.25, 0.5), (0.25, 0.5) and (0.25, 0.5) to improve experimental accuracy. The top view of the layout of sampling places is shown in Fig. 2, where totally 90 sampling points were included.

Flatbed scanning image analysis

Flatbed scanning can be utilized to present the real size of needle-shaped particles like biomass materials. As shown in Fig. 1a, d, vacuum dispersion device (VDD270, Occhio s.a., Angleur, Belgium) were employed to disperse MDF dust, where 5 mg of the particles for each sampling place were placed on a cylindrical chamber covered with polyethylene (PE) film. The air inside the chamber was pumped out, and the particles fell into the chamber and gently settled on the glass plate of the image analyzer (scan600, Occhio s.a., Angleur, Belgium) for image analysis once the vacuum level was low enough to destroy the PE film. The images of scanned samples were instantaneously analyzed by the built-in software CallistoEXPERT to calculate particle size and shape distribution (Fig. 1e).

Table 1 Milling parameters at three cutting speeds

Cutting width, mm	Cutting depth, mm	Spindle speed, rpm	Cutting speed, m/s	Feed rate, m/min	Total time of milling, min	Total volume of removed MDF, m^3
3	1	8000	3.351	3.394	105	9×10^{-4}
		12,000	5.027	5.091	75	
		16,000	6.702	6.788	61	

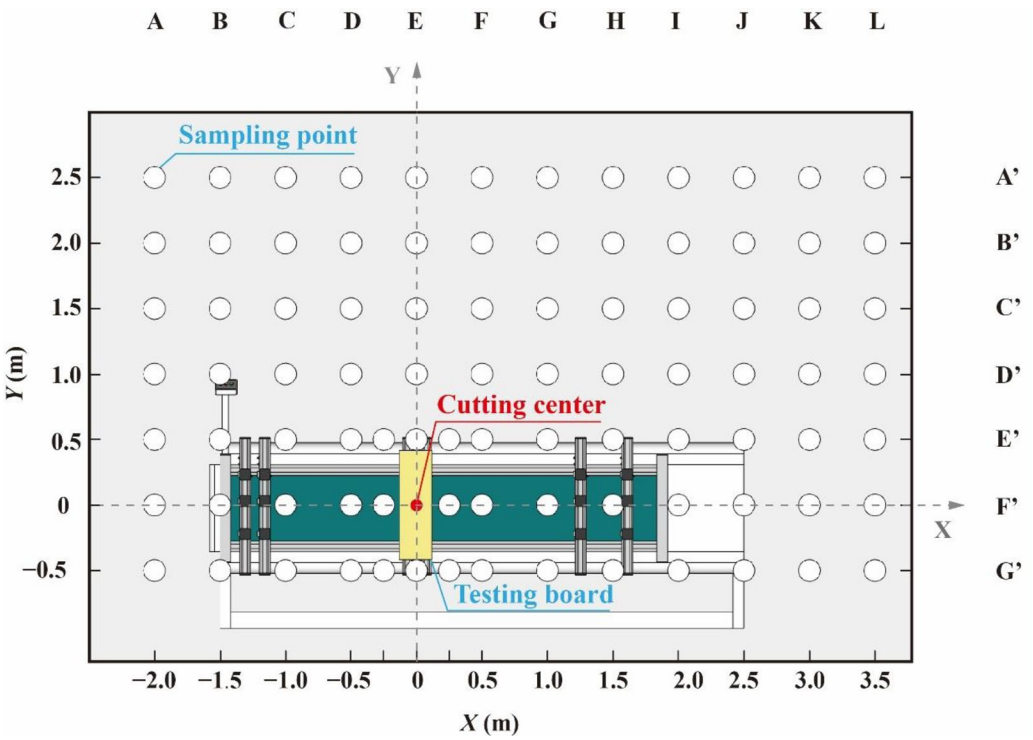

Fig. 2 Top view of workshop of MDF milling and layout of sampling points

Assuming that all particles had identical flatness ratios, the area-equivalent diameter was figured out by measuring the projected area of particles on the scanning plane according to Eq. 2:

$$d_{\mathrm{ae}}(\mu m) = 2\sqrt{\frac{A_p}{\pi}}, \tag{2}$$

where d_{ae} is the area-equivalent diameter (μm), A_{p} is the projected area of particles on the scanning plane calculated by software (μm^2) (Fig. 3).

PMSD can be converted from area-equivalent diameter, which is quite different from actual value since MDF dust particles are irregular. Although it is not commonly used in wood industry, PNSD can be more intuitive and accurate to reflect dust characteristic in image analysis compared to PMSD. Therefore, spatial PNSD of MDF dust was calculated in the present study. Usually, the dust particles smaller than 10 μm were less than 10% of all particles by mass [1]. However, a large quantity of such fine particles was still able to cause great damage in human health and equipment safety.

The shape of the particles is tightly correlated to the flowability of a dust [24]. Unlike metal materials and coal, MDF dust mainly composed of wood fibers has a larger length-to-width ratio. The particles with higher elongation have greater internal cohesion, resulting in the increase of the ability to resist external shear force and the decrease of flowability [25]. To describe particle

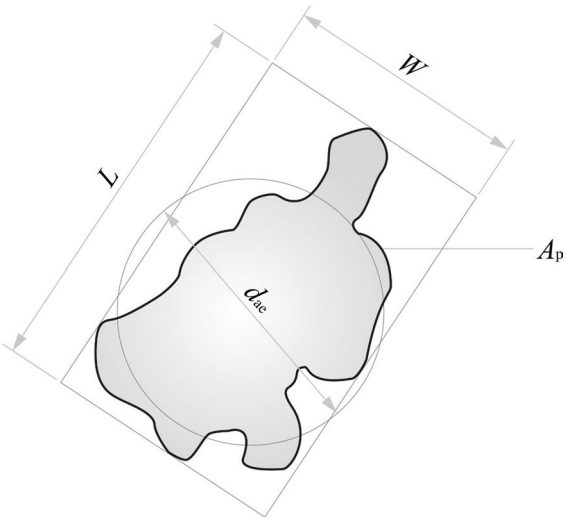

Fig. 3 The area, area-equivalent diameter, length and width of a particle projection

geometric proportion, the shape characteristics of MDF particle are quantified by AR, which was calculated by Eq. 3:

$$\mathrm{AR} = \frac{W}{L}, \tag{3}$$

where W is the width of the minimum box that contains the projected outline of a particle with the principal directions the same as the projection of the particle, and L is the length of the box (Fig. 3).

Scanning electron microscopy (SEM)

SEM together with image analysis can be used to measure particle size and distribution of airborne sanding dust [26]. Similarly, the particles obtained from the sampling points with spatial representativeness were in the oven till completely dried, and then they were coated with gold by a sputter coater (JFC 1600, JEOL Ltd, Tokyo, Japan) and placed in a SEM (JSM 7600F, JEOL Ltd, Tokyo, Japan) for photographing.

Results and discussion

Spatial distribution characteristics of MDF milling dust included spatial distribution of dust mass, spatial PNSD and spatial particle shape distribution. All of contour maps were generated by interpolation with the data in Additional file 1: Table S1–S18.

Spatial distribution of dust mass

The contour map of dust mass was drawn by measuring the net weight of the dust collected on the acrylic disc at every sampling place. No sampling places were located on the workpiece during milling, and the net weight of the dust in cutting center was defaulted to the maximum value of the scale, i.e., 10,000 mg. The contour maps displayed that the vast majority of the dust fell within a circular region centered on cutting origin with a radius of 0.5 m (Fig. 4). The regions embraced by various contour lines represented the areas for equal dust mass, among which the areas heavier than 12 mg were expanded with the increase of cutting speed, indicating that cutting speed spread the diffusion gradients of MDF dust. In contrast, the wood dust of 6 mg was scattered around, especially at cutting speed of 3.351 m/s, which might be due to lacking the interference of air turbulence at high cutting speeds.

Sampling places located on the same line were selected to representatively quantify the trend of dust mass distribution. When Y equaled 0, dust mass curves for the samplings on Line F' at different cutting speeds are displayed in Fig. 5. Dust mass reached up to the maximum around the cutting center, and it was asymmetrically decreased on both sides of cutting center. Obviously, the change in the right side ($X>0$) was slower than the other side ($X<0$), regardless of cutting speeds. When X was located at − 1.0 m, the dust mass was all below 10 mg, and almost maintained the constant level till the left end. In opposite direction, the dust mass was decreased to about 10 mg at 3 m away from the cutting center. Such directionality of dust mass distribution indicated the dust mainly flew to the positive direction of X-axis, which was 270° clockwise direction of the initial direction of cutting speed, suggesting there might be a relatively safe position for workers in milling MDF. Meanwhile, the higher the cutting speed, the more the dust mass accumulated in the direction of $X>0$. This might be caused by the particles having higher kinetic energy in the airflow with higher velocity resulting from higher cutting speeds, which traveled further in the rotating flow field.

Spatial particle number size distribution

The median sizes (the 50th percentile value) of MDF dust at three cutting speeds were very close, which were 25.138, 26.077 and 27.226 μm, respectively (Table 2). The mean sizes (33.338, 34.042 and 34.35 μm) were much higher than the median values, though they were also rather close to each other (Table 2), so were the standard deviations. The difference between median and mean sizes might be due to massive existence of relatively larger particles at the sampling places around the cutting center.

According to American Conference of Governmental Industrial Hygienists, PNSD identified by flatbed scanning image analysis can be divided into the respirable ($d_{ae}<10$ μm), thoracic ($d_{ae}<25$ μm) and inhalable ($d_{ae}<100$ μm) fractions [27]. Given that the dust with large size could cause damage to the equipment, the dust with $d_{ae}>100$ μm was also set as another fraction. The contours of four fractions of MDF dust at each sampling place are shown in Fig. 6. The dust dropping on the workpiece was sampled for analyzing the PNSD of the dust around the cutting center. The black areas missing data in contours resulted from less than 5 mg of the dust collected at the sampling place.

The contour map showed that the majority (more than 80.51%) of the MDF dust was smaller than 100 μm (Fig. 6a), which could be breathed into nose and mouth [28]. Similar result was obtained in wood sanding by Ding and Ockajova [29, 30]. The proportions of thoracic particles were from 30.87% to 67.84%, which was able to penetrate head airways and enter lung airways (Fig. 6b). Respirable fraction (97.14%–21.75%), known as PM_{10}, penetrated deeply into the respiratory tracts, including bronchial, bronchioles and the gas exchange region of the pulmonary alveoli [31] (Fig. 6c). Although the particles

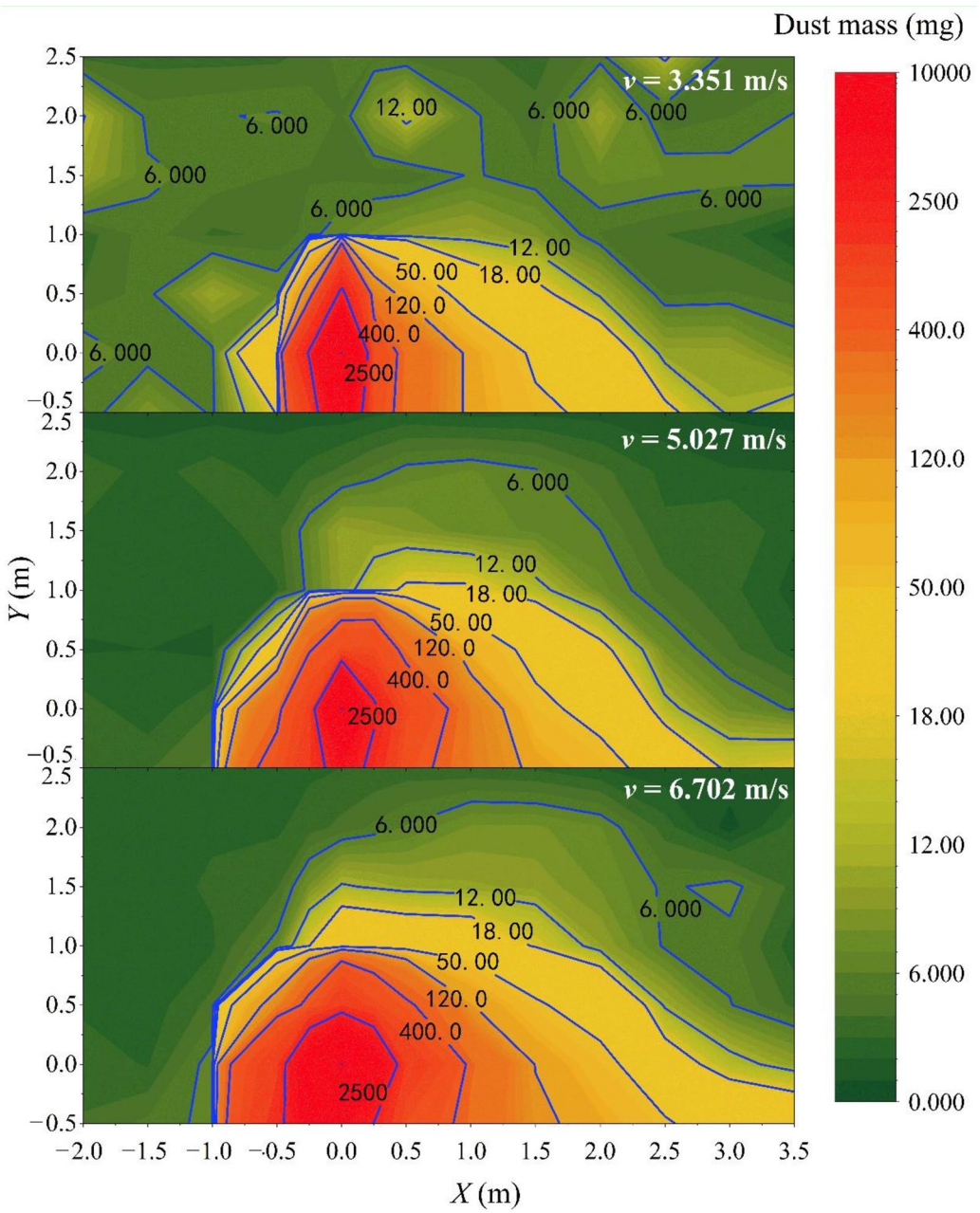

Fig. 4 The mass contour of dust particles collected from all sampling points at different cutting speeds

with $d_{ae} > 100$ μm accounted for a significant proportion in mass as reported in Chaloupkova's and Benthien's studies [16, 17], they only covered about 3.97% of all MDF dust (Fig. 6d).

Notably, regular regional heterogeneity existed in the quantitative proportion of four particle fractions. The concentration of fine dust close to cutting center was lower than the places far away from it. The amount of respirable, thoracic and inhalable fractions increased with the extension of X positive direction. For example, both respirable and thoracic fractions at the coordinates of (3.5, 0) were nearly twice as much as at cutting center (0, 0) under three cutting speeds. Moreover, the proportion of inhalable dust within 0.5 m around the cutting center was 19.17%, which was far lower than that of MDF sanding dust in Ding's study (99.6%) [29], whereas the

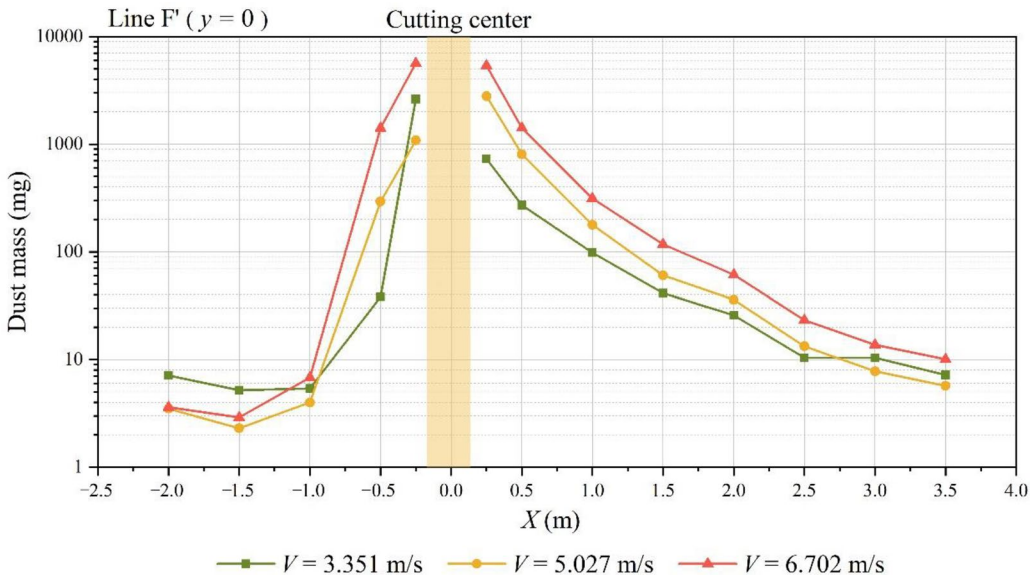

Fig. 5 The dust mass curves for dust particles collected from sampling points on Line F′ ($y=0$) at different cutting speeds

Table 2 The mean and median value of particle size and aspect ratio from all sampling points at three cutting speeds

Cutting speed, m/s	Particle size, μm		Aspect ratio	
	Mean	Median value	Mean	Median value
3.394	33.3 (14.6)	25.1 (6.5)	0.634 (0.016)	0.665 (0.008)
5.091	34.0 (11.9)	26.1 (6.4)	0.627 (0.018)	0.660 (0.012)
6.788	34.4 (11.5)	27.2 (6.0)	0.627 (0.015)	0.660 (0.010)

particles with $d_{ae} > 100$ μm, was only 19.49%, as shown in the lower left part of the contour map (Fig. 6d). Interestingly, for almost all fractions of particle sizes, the contour lines with the same value in the contour map preferably move toward the positive direction of X-axis with the increase of cutting speed.

To quantitatively compare PNSD at different places, three positions with an interval of 1 m were selected on the horizontal axis passing through the central point to create bar charts (Fig. 7), which displayed that MDF dust with the particle sizes of 20–30 μm accounted for the most proportion. The percentage for MDF particles lower than 30 μm increased continuously with the increase of the distance between the cutting center and the sampling points, whereas the particles larger than 30 μm had the opposite trend. Under all cutting speeds, cumulative curve at the position (0.5, 0) was smoother than the other two positions, suggesting that PNSD was more discrete near cutting center than in the areas farther away, where over 90% particles were less than 50 μm.

Cutting speed also affected PNSD at different positions as shown in Fig. 8. At the same sampling places, cutting speed was almost negatively correlated with the amount of the dust with d_{ae} less than 50 μm, but positively correlated with the dust with d_{ae} between 50 and 100 μm. The two fractions of dust with $d_{ae} < 50$ μm and d_{ae} from 50 to 100 μm at sampling point (0.5, 0) had more obvious changes with the increase of cutting speed compared with the other two sampling points.

Herein, it can be seen that PNSD was relevant to cutting speed and the distance from the cutting center both. The higher the spindle speed, the higher air velocity in the flow field and the more unstable the turbulence, and then the particles had a high initial velocity when they escaped from the MDF board in the case of high cutting speed. As a result, the dust with large particle sizes obtained a longer stride when falling into the ground due to the influence of gravity. Higher air velocity could cause dust re-entrainment, so that the dust with larger d_{ae} was moved from the position near cutting center to the other positions. Thus, there was a positive correlation between the cutting speed and PNSD dispersion at each position in the workshop, which was very obvious in the positive direction of X-axis.

Spatial particle shape distribution characteristics

As shown in Table 2, the AR of dust particle obtained by two-dimensional projection scanning were displayed as the mean of AR, which was a little lower than AR median. AR contours of all sampling points at different

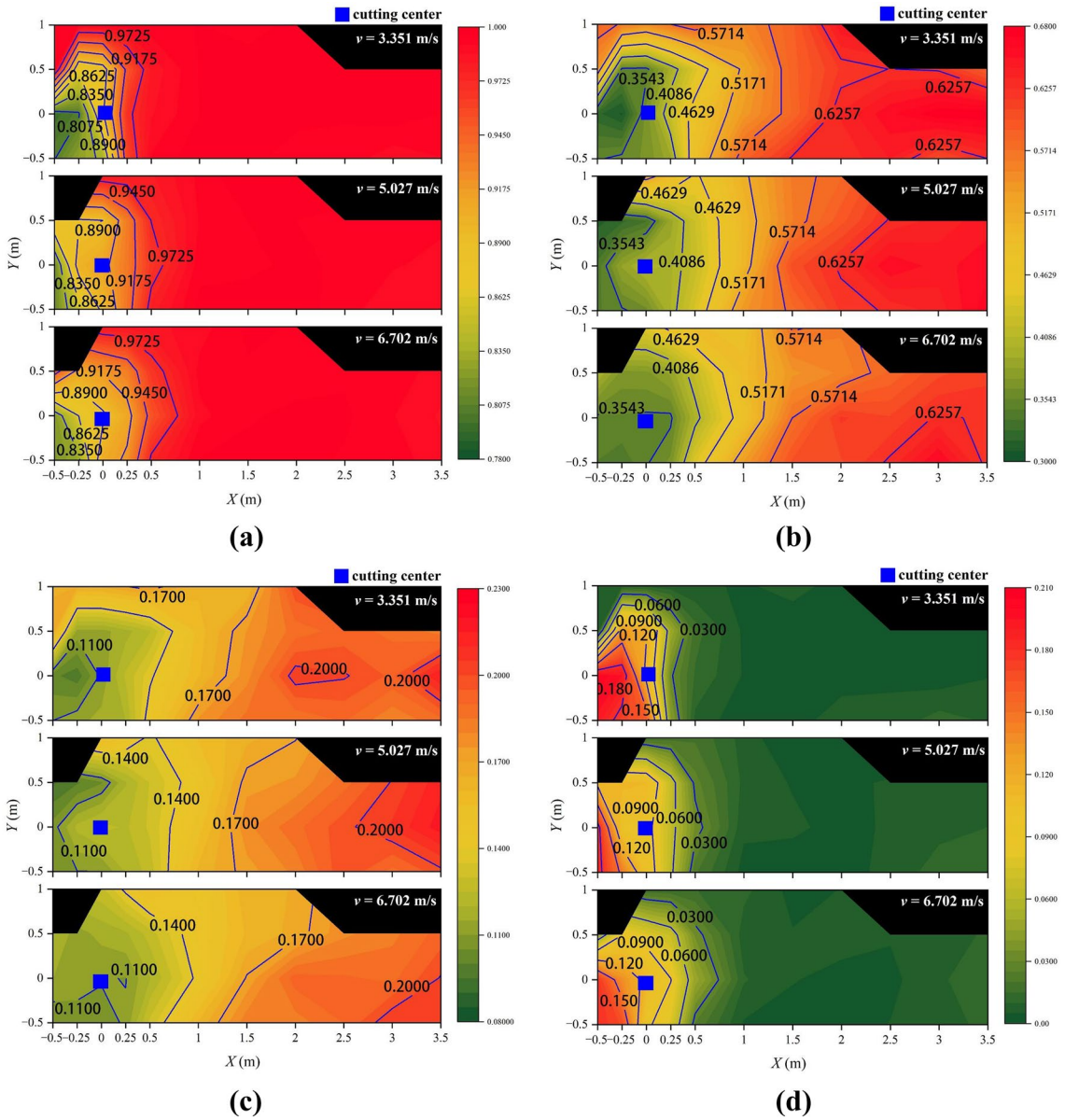

Fig. 6 The contour of number percentage of particles with **a** $d_{eq} < 100$ μm (the inhalable fraction); **b** $d_{eq} < 25$ μm (the thoracic fraction); **c** $d_{eq} < 10$ μm (the respirable fraction); **d** $d_{eq} > 100$ μm at different cutting speeds

cutting speeds are shown in Fig. 9. The area contained by the contour with equivalent levels of AR was increased with the increase of cutting speed where AR mean values was subtly varied between 0.60 and 0.66, corresponding to different sampling points. Although only a moderate variation in AR was found, the area contained in the contour for similar average value was augmented with the increase of cutting speed, which also suggested that AR mean was affected by cutting speed slightly.

Then AR distribution at the coordinates of (0.5, 0), (1.5, 0) and (2.5, 0) on Line F' was compared as shown in Fig. 10, where the percentage of quantity corresponding to a series of AR had similar tendency under different cutting speeds. The proportion of particles with AR between 0.65 and 0.75 accounted for 18.626–32.179%, which was at least 2 times higher than other particle groups attributed to the left-skewed distribution. The result revealed the reason why the AR mean was lower

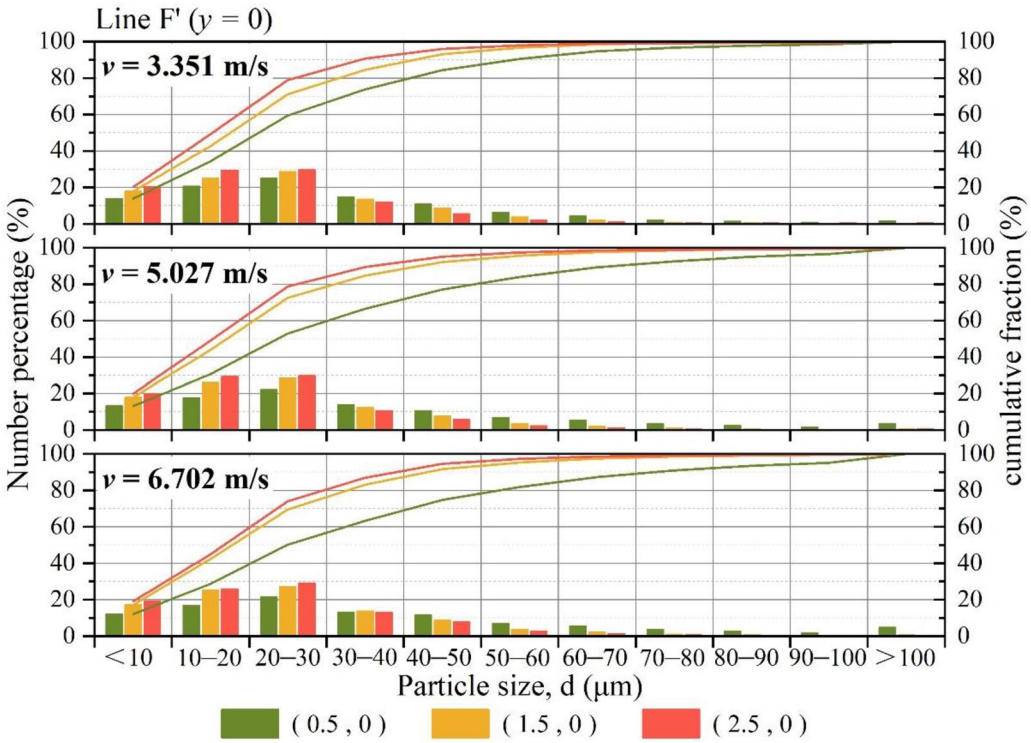

Fig. 7 The PNSD of dust particles collected from sampling points at the coordinates of (0.5, 0), (1.5, 0) and (2.5, 0)

than AR median. The AR values of MDF sanding particles less than 10 μm ranged between 0.7 and 0.8, which was consistent with previous report [29]. AR distribution was relatively uniform in the range of 0.45–0.65 and very few particles were found when AR was less than 0.2 or more than 0.9. Notably, AR distribution was significantly influenced by the distance away from the cutting center. The farther away from the cutting center the sampling point, the more the dust with AR between 0.65 and 0.75, and vice versa, which might result from the high proportion of small particles in size.

Regression analysis was performed to define the variations in average particle size and AR with the change of X-axis coordinates on line F' as shown in Fig. 11. Under different cutting speeds, average particle size was decreased in a quadratic negative correlation with the distance from the cutting center, whereas AR was proportionally correlated with the range. The regression equations for smooth curves fitted to the change of average particle size at different cutting speeds were displayed as follows, respectively:

$$y = 58.91 - 7.620x + 0.364x^2 (v = 3.351 \text{ m/s}),$$

$$y = 83.352 - 13.363x + 0.703x^2 (v = 5.027 \text{ m/s}),$$

$$y = 102.995 - 17.906x + 0.972x^2 (v = 6.702 \text{ m/s}).$$

The regression lines of AR at different cutting speeds were crossed at the end of X positive direction, suggesting that the effect of cutting speed on AR was not significant, which were also presented in the following equations, separately:

$$y = 0.580 + 0.007x (v = 3.351 \text{ m/s}),$$

$$y = 0.538 + 0.012x (v = 5.027 \text{ m/s}),$$

$$y = 0.564 + 0.009x (v = 6.702 \text{ m/s}).$$

Importantly, the smaller the particles generated during MDF milling, the more even the shape to a certain

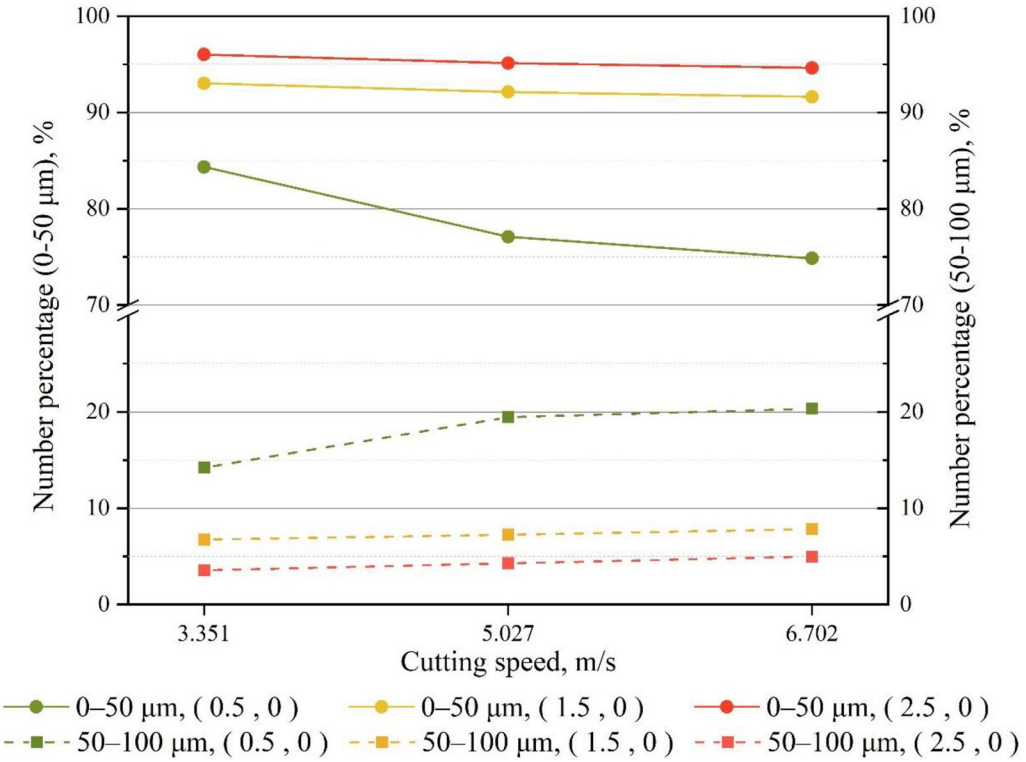

Fig. 8 The relationship between cutting speed and proportion of particles with d_{eq} of 0–50 μm and 50–100 μm collected at the coordinates of (0.5, 0), (1.5, 0) and (2.5, 0)

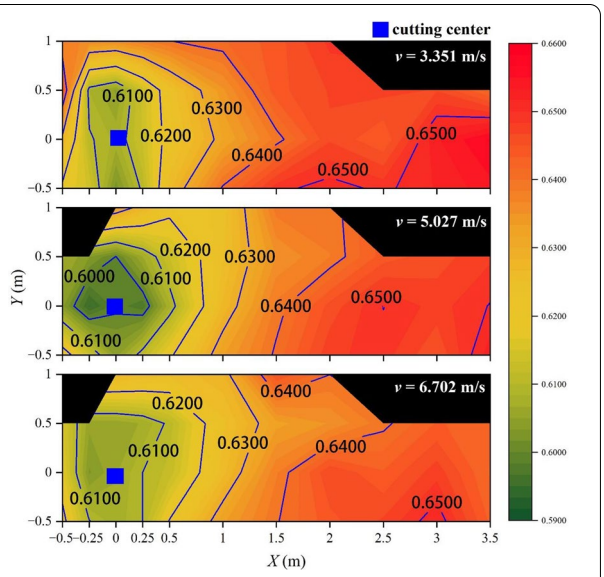

Fig. 9 The contour map of mean AR of dust particles collected from the indicated sampling points at different cutting speeds

extent, i.e., the reduction of MDF dust in size gradually decreased the discrepancy of MDF dust in shape and made them more homogeneous. This was also consistent with bio-based particles in previous studies [20, 32, 33].

SEM analysis was also carried out to check the shape of particles, and the SEM image of the most typical particle is shown in Fig. 12a. The d_{eq} was approximately 35 μm and AR was 0.71. A massive number of such particles existed in whole space, which became the maximum amount of particles produced in MDF milling. They were morphologically different from wood fiber, which are more like the chemical components of MDF panel, such as urea formaldehyde resin and the combination of chemical additives and wood fiber derived from the MDF panel. Most of the fiber bundles were fractured after tool extrusion as shown in Fig. 12b. The fiber was usually about 1 mm in length, and the broken fiber was 100 μm or so, close to the average cutting thickness of 0.05 mm, which proved the damage of the cutting tool to the fiber.

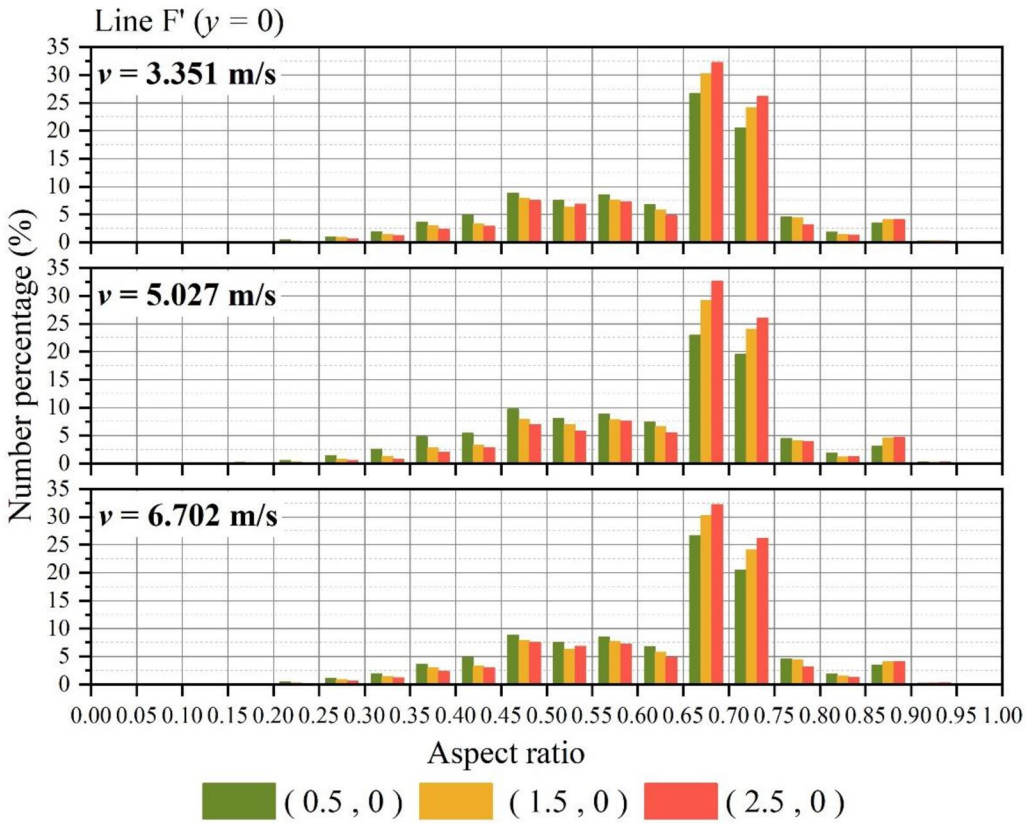

Fig. 10 The aspect ratios of dust particles collected from sampling points at the coordinates of (0.5, 0), (1.5, 0) and (2.5, 0)

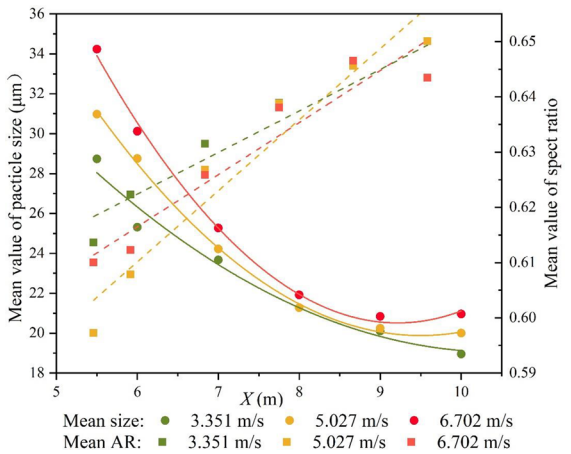

Fig. 11 The means of particle sizes and aspect ratios showed the opposite trend with the increase of *X* value

Conclusions

In the study, the mass, PNSD and AR of the dust generated in workshop during MDF milling were investigated by weighting, flatbed scanning image analysis and scanning electron microscopy. We found the majority of MDF dust spread in the direction of 270° clockwise of initial direction of cutting speed (positive axis of X). There were significant differences for PNSD at different positions. The amount of fine dust far from cutting center was more than that around cutting center. Similarly, AR distribution was significantly affected, i.e., the farther away from the cutting center, the more concentrated the AR value of dust. The higher the cutting speed, the less the amount of fine dust far away from cutting center. The total amount of dust was increased with the augment of cutting speed, while cutting speed did not have significant effect on AR. The positions

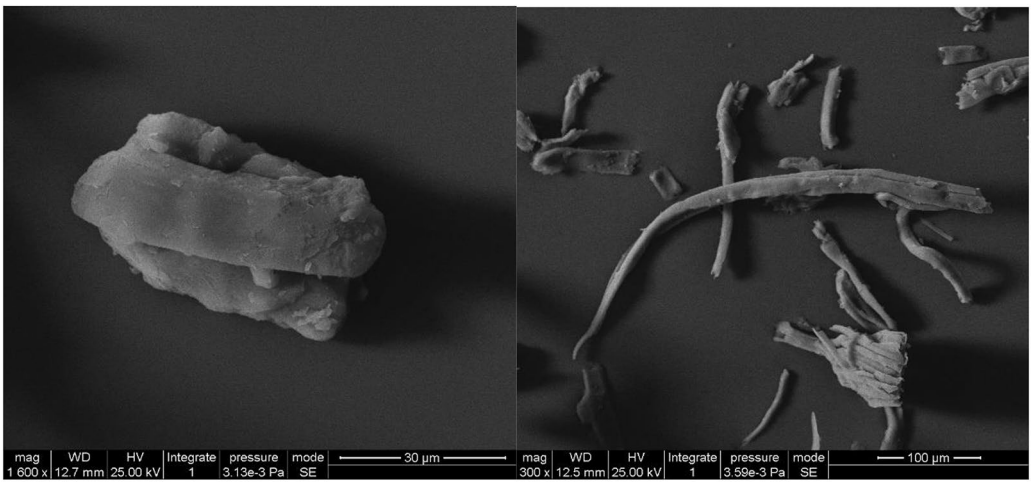

Fig. 12 The SEM images of dust particles. **a** The most typical particle with $d_{eq} = 35$ µm and AR = 0.71; **b** fiber bundles fractured by tool extrusion

in the negative X direction near cutting center due to lower mass of dust and less proportion of respirable dust might be the most suitable location for operators. Conversely, installing dust collecting hoods in positive X direction could improve the efficiency of dust removal. These findings for spatial distribution characteristics of MDF dust might provide a theoretical basis to better MDF dust control in wood processing industry and offered constructive strategies for reducing harmful dust to humans and equipment by optimizing cutting parameters and location of operators.

Abbreviations

MDF: Medium-density fiberboard; UF: Urea formaldehyde; PMSD: Particle mass size distribution; PNSD: Particle number size distribution; IA: Image analysis; SEM: Scanning electron microscopy; AR: Aspect ratio.

Supplementary Information

The online version contains supplementary material available at https://doi.org/10.1186/s10086-022-02025-6.

Additional file 1. The actual value obtained at each sampling point in the experiment.

Acknowledgements

The authors acknowledge the help of the Advanced Analysis and Testing Center of Nanjing Forestry University.

Authors' contributions

YC analyzed the experimental data and drafted the manuscript. YC, JY, YT and HW performed the experiments and prepared the figures. DT is the project leader and responsible for the experimental design and manuscript review. NZ provided the experimental equipments and contributed to the image analysis. All authors read and approved the final manuscript.

Funding

The authors gratefully acknowledge the financial support from the National Key R&D Program of China (No. 2016YFD0600703).

Availability of data and materials

The datasets used and/or analyzed during the current study are available from the corresponding author on reasonable request.

Declarations

Competing interests

The authors declare that they have no competing interests.

Received: 17 November 2021 Accepted: 8 March 2022
Published online: 17 March 2022

References

1. Chung KYK, Cuthbert RJ, Revell GS, Wassel SG, Summers N (2000) A study on dust emission, particle size distribution and formaldehyde concentration during machining of medium density fibreboard. Ann Occup Hyg 44(6):455–466. https://doi.org/10.1016/S0003-4878(00)00005-3
2. Ayrilmis N (2007) Effect of panel density on dimensional stability of medium and high density fiberboards. J Mater Sci 42(20):8551–8557. https://doi.org/10.1007/s10853-007-1782-8
3. Food and Agriculture Organization of the United Nations (2019) FAO yearbook of forest products 2018. FAO, Geneva. ISBN 978-92-5-133127-9. https://www.fao.org/forestry/statistics/80570/en/?utm_source=usbstick&utm_medium=qrcode&utm_campaign=forestyearbook
4. Palmqvist J, Gustafsson SI (1999) Emission of dust in planing and milling of wood. Holz als Roh- und Werkstoff 57(3):164–170. https://doi.org/10.1007/s001070050035
5. Calle S, Klaba L, Thomas D, Perrin L, Dufaud O (2005) Influence of the size distribution and concentration on wood dust explosion: experiments and reaction modelling. Powder Technol 157(1–3):144–148. https://doi.org/10.1016/j.powtec.2005.05.021
6. Pang ZH, Zhu NF, Cui YQ, Li WZ, Xu CY (2020) Experimental investigation on explosion flame propagation of wood dust in a semi-closed tube. J Loss Prev Process Ind 63:10. https://doi.org/10.1016/j.jlp.2019.104028
7. Yepes MEG, Cremades LV (2011) Characterization of wood dust from furniture by scanning electron microscopy and energy-dispersive X-ray

analysis. Ind Health 49(4):492–500. https://doi.org/10.2486/indhealth.MS1204
8. Jacobsen G, Schaumburg I, Sigsgaard T (2010) Non-malignant respiratory diseases and occupational exposure to wood dust. Part I. Fresh wood and mixed wood industry. Ann Agric Environ Med 17(1):15. https://doi.org/10.1007/s13280-010-0046-z
9. Nylander LA, Dement JM (1993) Carcinogenic effects of wood dust: review and discussion. Am J Ind Med 24(5):619–647. https://doi.org/10.1002/ajim.4700240511
10. GUO (2010) Effect of average chip thickness on dust particle size and surface roughness. JAnhui Agri Sci 38 (19):10078–10080+10241. https://doi.org/10.3969/j.issn.0517-6611.2010.19.055
11. Zhu ZL, Buck D, Ekevad M, Marklund B, Guo XL, Cao PX, Zhu NF (2019) Cutting forces and chip formation revisited based on orthogonal cutting of Scots pine. Holzforschung 73(2):131–138. https://doi.org/10.1515/hf-2018-0037
12. Pedzik M, Stuper-Szablewska K (2020) Influence of grit size and wood species on the granularity of dust particles during sanding. Appl Sci 10(22):8165. https://doi.org/10.3390/app10228165
13. Fu XW, Huck D, Makein L, Armstrong B, Willen U, Freeman T (2012) Effect of particle shape and size on flow properties of lactose powders. Particuology 10(2):203–208. https://doi.org/10.1016/j.partic.2011.11.003
14. Ganesan V, Rosentrater KA, Muthukurnarappan K (2008) Flowability and handling characteristics of bulk solids and powders - a review with implications for DDGS. Biosys Eng 101(4):425–435. https://doi.org/10.1016/j.biosystemseng.2008.09.008
15. Okajová A, Barcik S, Kucerka M (2019) Wood dust granular analysis in the sanding process of thermally modified wood versus its density. BioResources 14(4):8559–8572. https://doi.org/10.15376/biores.14.4.8559-8572
16. Okajová A, Stebila J, Rybakowski M (2014) The granularity of dust particles when sanding wood and wood-based materials. Adv Mater Res 1001:432–437. https://doi.org/10.4028/www.scientific.net/AMR.1001.432
17. Mazumder KM (1997) aerodynamic properties and respiratory deposition characteristics of formaldehyde impregnated medium-density fiberboard particles. Part Sci Technol 15(1):37–49. https://doi.org/10.1080/02726359708906708
18. Lee YJ, Yoon WB (2015) Flow behavior and hopper design for black soybean powders by particle size. J Food Eng 144:10–19. https://doi.org/10.1016/j.jfoodeng.2014.07.005
19. Gil M, Teruel E, Arauzo I (2014) Analysis of standard sieving method for milled biomass through image processing. Effects of particle shape and size for poplar and corn stover. Fuel 116:328–340. https://doi.org/10.1016/j.fuel.2013.08.011
20. Saad M, Sadoudi A, Rondet E, Cuq B (2011) Morphological characterization of wheat powders, how to characterize the shape of particles? J Food Eng 102(4):293–301. https://doi.org/10.1016/j.jfoodeng.2010.08.020
21. Igathinathane C, Pordesimo LO, Columbus EP, Batchelor WD, Sokhansanj S (2009) Sieveless particle size distribution analysis of particulate materials through computer vision. Comput Electron Agric 66(2):147–158. https://doi.org/10.1016/j.compag.2009.01.005
22. Benthien JT, Heldner S, Ohlmeyer M (2018) Size distribution of wood particles for extruded particleboard production determined by sieve analysis and image analysis-based particle size measurement. Eur J Wood Wood Prod 76(1):375–379. https://doi.org/10.1007/s00107-017-1215-6
23. Rautio S, Hynynen P, Welling I, Hemmilä P, Usenius A, Närhi P (2007) Modelling of airborne dust emissions in CNC MDF milling. Holz als Roh- und Werkstoff 65(5):335–341. https://doi.org/10.1007/s00107-007-0179-3
24. Rezaei H, Lim CJ, Lau A (2016) Size, shape and flow characterization of ground wood chip and ground wood pellet particles. Powder Technol 301:737–746. https://doi.org/10.1016/j.powtec.2016.07.016
25. Cleary V, Bowen P, Witlox H (2007) Flashing liquid jets and two-phase droplet dispersion I. Experiments for derivation of droplet atomisation correlations. J Hazard Mater 142(3):786–796. https://doi.org/10.1016/j.jhazmat.2006.06.125
26. Mazzoli A, Favoni O (2012) Particle size, size distribution and morphological evaluation of airborne dust particles of diverse woods by Scanning Electron Microscopy and image processing program. Powder Technol 225:65–71. https://doi.org/10.1016/j.powtec.2012.03.033
27. American Conference of Governmental Industrial Hygienists (ACGIH) (2015) 2015 TLVs and BEIs (Threshold Limit Values for Chemical Substances and Physical Agents & Biological Exposure Indices) Cincinnati, OH, USA. ISBN: 978-1-607260-77-6
28. Gu J, Kirsch I, Schripp T, Froning-Ponndorf F, Berthold D, Salthammer T (2018) Human exposure to airborne particles during wood processing. Atmos Environ 193:101–108. https://doi.org/10.1016/j.atmosenv.2018.08.064
29. Ding T, Zhao JF, Zhu NF, Wang CM (2020) A comparative study of morphological characteristics of medium-density fiberboard dust by sieve and image analyses. J Wood Sci 66(1):9. https://doi.org/10.1186/s10086-020-01896-x
30. Okajová A, Kuerka M, Kminiak R (2020) Granulometric composition of chips and dust produced from the process of working thermally modified wood. Acta Facultatis Xylologiae 62(1):103–111. https://doi.org/10.17423/afx.2020.62.1.09
31. Oberdoester G (2005) Nanotoxicology: an emerging discipline evolving from studies of ultrafine particles. Environ Health Perspect 113(7):823–839. https://doi.org/10.1289/ehp.7339
32. Guo Q, Chen X, Liu H (2012) Experimental research on shape and size distribution of biomass particle. Fuel 94:551–555. https://doi.org/10.1016/j.fuel.2011.11.041
33. Lu Z, Hu X, Lu Y (2017) Particle morphology analysis of biomass material based on improved image processing method. Int J Anal Chem 2017:5840690. https://doi.org/10.1155/2017/5840690

Publisher's Note